PHYSICAL REVIEW A **94**, 043833 (2016)

Stationary light pulses and narrowband light storage in a laser-cooled ensemble loaded into a hollow-core fiber

Frank Blatt,[1] Lachezar S. Simeonov,[2] Thomas Halfmann,[1] and Thorsten Peters[1]
[1]*Institut für Angewandte Physik, Technische Universität Darmstadt, Hochschulstraße 6, 64289 Darmstadt, Germany*
[2]*Department of Physics, Saint Kliment Ohridski University of Sofia, 5 James Bourchier Boulevard, 1164 Sofia, Bulgaria*
(Received 18 March 2016; published 19 October 2016)

We report on an observation of stationary light pulses and narrowband light storage inside a hollow-core photonic crystal fiber. Laser-cooled atoms were first loaded into the fiber core, providing strong light-matter coupling. Light pulses were then stored in a collective atomic excitation using a single control laser beam. By applying a second counterpropagating control beam, a light pulse could be brought to a standstill. Our work paves the way towards the creation of strongly correlated many-body systems with photons and applications in the field of quantum information processing.

DOI: 10.1103/PhysRevA.94.043833

I. INTRODUCTION

Achieving strong coupling of light and matter is a long pursued goal in the field of quantum optics. Not only does it allow for large linear light storage efficiencies [1], e.g., using electromagnetically induced transparency (EIT) [2–4] or gradient-echo techniques [5,6]. It also enables quantum nonlinear optics (NLO), with strong interactions between *individual* photons mediated via couplings through the medium [7].

In particular EIT has drawn a lot of attention and led to, e.g., impressive light storage times [8] and efficiencies [9]. EIT is implemented in a coupling scheme as shown in Fig. 1(a). In this Λ-type system the strong control field renders an opaque medium transparent for the weak (copropagating) probe field due to quantum interference near two-photon resonance at $\Delta_p = \Delta_c$. Dark-state polaritons (DSPs) [10] are formed. Their group velocity can be controlled by the control Rabi frequency Ω_c [11]. By adiabatically switching off the control field while the DSPs are created, we map the probe field onto a stationary long-lived collective atomic excitation, i.e., atomic coherences. We can retrieve the probe field again from the collective excitation by reapplying the control field to beat with the atomic coherences. This is termed light storage and retrieval [8,12].

When we add a second counterpropagating control beam [see Fig. 1(b)] while the DSPs propagate through the medium, the latter acts like an all-optical cavity for the probe pulse. The DSPs are effectively stopped with a nonvanishing photonic component and a quasistationary envelope [13,14], hence the term *stationary light pulses* (SLPs). Although the envelope is quasistationary, the DSPs within the pulse still jitter back and forth with finite group velocity. With a Kerr-type coupling being present this results in (in)elastic collisions of the DSPs, depending on the magnitude of the detunings from the atomic resonances [15]. Thus, NLO interactions using SLPs become possible [16,17]. This could enable, e.g., strongly correlated light-matter systems [18–20], single-photon switches [15], all-optical quantum networks [21], or the simulation of relativistic theories with photons [22].

The manipulation of optically linear effects (i.e., absorption and dispersion) by EIT relies on a strong coupling of the probe field to the atomic ensemble. The coupling strength of light to an ensemble of N_{atom} atoms is determined by the optical depth $D_{\mathrm{opt}} = -\ln T$, with the resonant transmission T [1]. Thus, efforts are being made to increase the D_{opt}, e.g., using multipass setups [4] or creating large laser-cooled atomic ensembles [23]. Large light storage efficiencies were recently demonstrated with the latter system [9].

Although highly efficient linear interactions are nowadays possible, nonlinear interactions at the few-photon level are yet difficult to achieve as the simultaneous interaction of an atom with multiple photons is required. Successful NLO interactions at the quantum level were demonstrated, e.g., using long-range atom-atom interactions [24–27] or placing atoms into high-finesse cavities [28,29]. However, those NLO interactions based on SLPs as proposed in [15,18–20,22] using atomic ensembles coupled to one-dimensional (1D) waveguides are still waiting for their experimental realization. The difficulties arise here from creating not only large D_{opt} as required for linear interactions, but also to realize a large D_{opt} per atom, $D^*_{\mathrm{opt}} = D_{\mathrm{opt}}/N_{\mathrm{atom}} \approx \sigma_a/A_w$, which represents the probability of an atom (absorption cross section σ_a) to interact with a photon of the guided mode (mode area A_w) [7]. The quantity that has to be maximized for efficient NLO interaction is the product $D_{\mathrm{opt}} \times D^*_{\mathrm{opt}}$ [15]. Progress was achieved with atoms coupled to photonic nanowaveguides yielding $D^*_{\mathrm{opt}} \approx 2$ for $D_{\mathrm{opt}} \approx 5$ [30,31] and with nanofibers [32] yielding $D^*_{\mathrm{opt}} \approx 0.027$ for $D_{\mathrm{opt}} \approx 28$ [33]. On the other hand, hollow-core photonic crystal fibers (HCPCFs) loaded with atoms [34–37] provide a smaller $D^*_{\mathrm{opt}} \approx 0.004$ [37,38] due to a larger mode area but allow for significantly larger D_{opt} [34,37–39]. HCPCFs filled with (above-)room-temperature atoms so far provide the

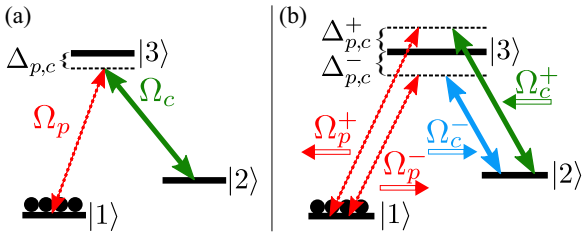

FIG. 1. Coupling schemes for EIT (a) and SLPs (b). $\Omega_{p,c}$ are the Rabi frequencies of the probe and control fields, respectively.

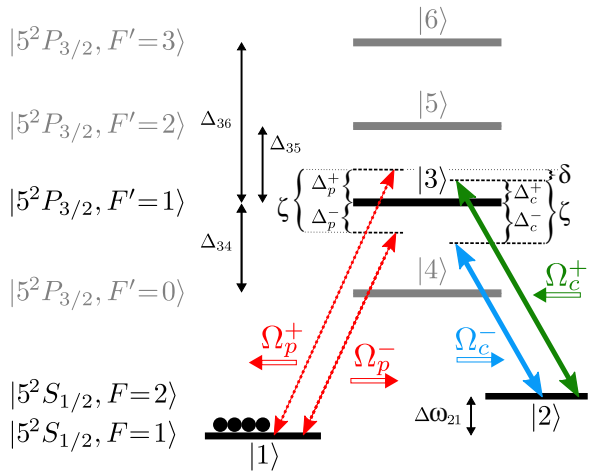

FIG. 2. Level scheme of ^{87}Rb used for the simulation of transmission and propagation.

largest D_{opt} [39,40], however, at the expense of short coherence times due to transit relaxation decay by frequent collisions of the atoms with the fiber wall and/or lower D^*_{opt} due to larger core dimensions. Broadband EIT [34] and broadband light storage and retrieval [41] were already observed in such systems. In order to achieve narrowband EIT, light storage and retrieval, and SLPs, with these fibers, HCPCFs have to be loaded with laser-cooled atoms [35,36,38,42]. Narrowband EIT and slow light were first demonstrated by Bajcsy *et al.* [42] with such a setup at $D^*_{\mathrm{opt}} \approx 0.01$ and $D_{\mathrm{opt}} \lesssim 30$.

Here we present the experimental implementation of narrowband EIT in a cold 1D ensemble with large optical depth up to $D_{\mathrm{opt}} = 400$ at $D^*_{\mathrm{opt}} \approx 0.004$, and the first demonstration of narrowband light storage and retrieval inside a HCPCF. Towards the goal of implementing efficient fiber-based linear and NLO interactions at the quantum level, we also present the first observation of SLPs in a HCPCF. We compare our results to elaborated numerical simulations. Finally we discuss strategies towards future applications.

II. THEORETICAL DESCRIPTION

In order to compare our measurements to theoretical predictions and to characterize our setup we set up several numerical simulations. We extended the theoretical models typically used to simulate the transmission through a fiber loaded with atoms [37] and pulse propagation in a medium driven by EIT with counterpropagating control fields [43–45] to incorporate also off-resonant states. This is necessary, as for $D_{\mathrm{opt}} \gtrsim 130$ the resonances of the D_2 line used start to overlap. Also, inhomogeneous broadening of the two-photon resonance due to radially inhomogeneous control fields $\Omega_c(r)$ and the atomic density profile $n(r)$ determined by the trap potential inside the fiber and the temperature of the atoms Θ [46] have to be considered.

A. Hamiltonian

We consider the level scheme corresponding to the D_2 line of ^{87}Rb with degenerate Zeeman states shown in Fig. 2 with $\Delta_{3i} = \omega_i - \omega_3$ being the frequency difference between states $|i\rangle$ and $|3\rangle$. The system is driven by two strong counterpropagating control fields of Rabi frequencies $\Omega_c^{\pm}$ detuned from the transition $|5\,^2S_{1/2}, F = 2\rangle \rightarrow |5\,^2P_{3/2}, F' = 1\rangle$ by $\Delta_c^{\pm} = \omega_c^{\pm} - (\omega_3 - \omega_2)$. A weak probe field E_p^+ of Rabi frequency Ω_p^+ and detuned from the transition $|5\,^2S_{1/2}, F = 1\rangle \rightarrow |5\,^2P_{3/2}, F' = 1\rangle$ by $\Delta_p^+ = \omega_p^+ - (\omega_3 - \omega_1)$ is sent into the medium propagating into the forward direction. Upon interaction with the two counterpropagating control fields, another probe field E_p^- traveling into the backward direction is created in a four-wave mixing process with Rabi frequency Ω_p^- and $\Delta_p^- = \Delta_p^+ - \Delta_c^+ + \Delta_c^-$ due to energy conservation. All six levels of the atomic structure are taken into account with level $|5\,^2P_{3/2}, F' = 3\rangle$ being adiabatically eliminated.

The Hamiltonian reads

$$\begin{aligned}\hat{H} = {} & \hbar(\omega_p^+ - \omega_c^+ - \Delta_p^+ + \Delta_c^+)|2\rangle\langle 2| \\ & + \hbar(\omega_p^+ - \Delta_p^+)|3\rangle\langle 3| + \hbar(\omega_p^+ - \Delta_p^+ + \Delta_{34})|4\rangle\langle 4| \\ & + \hbar(\omega_p^+ - \Delta_p^+ + \Delta_{35})|5\rangle\langle 5| + \hat{V}, \end{aligned} \tag{1}$$

where $\hat{V}$ is the interaction part with the electromagnetic field,

$$\begin{aligned} -\frac{2}{\hbar}\hat{V} = {} & e^{-i\omega_p^+ t}\sum_{\mu=3}^{5}\left(\Omega_p^{+(1\mu)}e^{ikz} + \Omega_p^{-(1\mu)}e^{-i\zeta t - ikz}\right)|\mu\rangle\langle 1| \\ & + e^{-i\omega_c^+ t}\sum_{\mu=3}^{5}\left(\Omega_c^{+(2\mu)}e^{ikz} + \Omega_c^{-(2\mu)}e^{-i\zeta t - ikz}\right)|\mu\rangle\langle 2| \\ & + \mathrm{H.c.}, \end{aligned} \tag{2}$$

with $\zeta \equiv \Delta_c^- - \Delta_c^+ = \Delta_p^- - \Delta_p^+$, $\Omega_c^{\pm(24)} = 0$ due to selection rules, and $k = k_c \approx k_p$ is the wave vector of the control field. $\Omega_p^{\pm(1\mu)}$ denote the probe beam Rabi frequencies of the fields traveling along the $\pm z$ direction. The superscripts (1μ) imply that the probe electric field E_p is multiplied with the corresponding normalized relative hyperfine transition strength factors $\tilde{S}_{1\mu} = \sqrt{S_{1\mu}/S_{13}}$ [47] for the transition $|1\rangle \leftrightarrow |\mu\rangle$, normalized to the transition $|1\rangle \leftrightarrow |3\rangle$. Thus, we assume unpolarized excitation using effective dipole moments [see Eq. (43) in Ref. [47]] due to a changing elliptical light polarization inside the HCPCF and a potentially small remaining magnetic field. The same applies to the control beam Rabi frequencies $\Omega_c^{\pm(2\mu)}$ with $\tilde{S}_{2\mu} = \sqrt{S_{2\mu}/S_{23}}$ [47] normalized to the transition $|2\rangle \leftrightarrow |3\rangle$. For simplicity we use below the notation $\Omega_p^{\pm(13)} \equiv \Omega_p^{\pm}$ as well as $\Omega_c^{\pm(23)} \equiv \Omega_c^{\pm}$, as the near-resonant transitions in our experiments are $|1\rangle \leftrightarrow |3\rangle \leftrightarrow |2\rangle$. State $|5\,^2P_{3/2}, F' = 3\rangle$ is adiabatically eliminated and appears in the form of a Stark shift:

$$\Delta_S = \Delta_S^+ + \Delta_S^- \quad \text{with} \quad \Delta_S^{\pm} = -\frac{\left|\Omega_c^{\pm(26)}\right|^2}{4(\Delta_{36} - \Delta_c^{\pm})}. \tag{3}$$

For convenience we neglect this Stark shift in the following, but it will be included later on by appropriate redefinition of the detunings $\Delta_c^{\pm}$.

B. Pulse propagation

The relevant Bloch equations [44] of the five-level system considering selection rules are then given by

$$\frac{\partial}{\partial t}\rho_{21} = -\left[\frac{\gamma_{21}}{2} - i\delta\right]\rho_{21} + \frac{i}{2}(\Omega_c^{+*}e^{-ikz} + \Omega_c^{-*}e^{i\zeta t+ikz})\rho_{31} + \frac{i}{2}\left(\Omega_c^{+(25)*}e^{-ikz} + \Omega_c^{-(25)*}e^{i\zeta t+ikz}\right)\rho_{51}, \quad (4)$$

$$\frac{\partial}{\partial t}\rho_{31} = -\left[\frac{\Gamma}{2} - i\Delta_p^{+}\right]\rho_{31} + \frac{i}{2}(\Omega_p^{+}e^{ikz} + \Omega_p^{-}e^{-i\zeta t-ikz}) + \frac{i}{2}(\Omega_c^{+}e^{ikz} + \Omega_c^{-}e^{-i\zeta t-ikz})\rho_{21}, \quad (5)$$

$$\frac{\partial}{\partial t}\rho_{41} = -\left[\frac{\Gamma}{2} - i(\Delta_p^{+} - \Delta_{34})\right]\rho_{41} + \frac{i}{2}\left(\Omega_p^{+(14)}e^{ikz} + \Omega_p^{-(14)}e^{-i\zeta t-ikz}\right), \quad (6)$$

$$\frac{\partial}{\partial t}\rho_{51} = -\left[\frac{\Gamma}{2} - i(\Delta_p^{+} - \Delta_{35})\right]\rho_{51} + \frac{i}{2}\left(\Omega_p^{+(15)}e^{ikz} + \Omega_p^{-(15)}e^{-i\zeta t-ikz}\right) + \frac{i}{2}\left(\Omega_c^{+(25)}e^{ikz} + \Omega_c^{-(25)}e^{-i\zeta t-ikz}\right)\rho_{21}. \quad (7)$$

Here, ρ_{jk} are the matrix elements of the density matrix $\langle j|\hat{\rho}|k\rangle$ between the atomic energy states $|j\rangle$ and $|k\rangle$, γ_{21} is the ground-state decoherence rate, Γ is the excited-state decay rate, and $\delta = \Delta_p^{\pm} - \Delta_c^{\pm}$ is the two-photon detuning (according to sending the pulses into the medium with a forward control field). We use $\rho_{11}^{(0)} = 1$ and $\rho_{ij}^{(0)} = 0$ for all $(i,j) \neq (1,1)$ as initial conditions, i.e., all population is in state $|1\rangle$.

Next, we expand the coherences into spatial Fourier components [43,44]

$$\rho_{21} = \sum_{n=-\infty}^{+\infty} \rho_{21}^{(2n)} e^{in\zeta t+i2nkz}, \quad (8)$$

$$\rho_{31} = \sum_{n=0}^{\infty} \rho_{31}^{(2n+1)} e^{in\zeta t+i(2n+1)kz} + \sum_{n=-\infty}^{0} \rho_{31}^{(2n-1)} e^{i(n-1)\zeta t+i(2n-1)kz}, \quad (9)$$

$$\rho_{41} = \rho_{41}^{(+1)} e^{ikz} + \rho_{41}^{(-1)} e^{-i\zeta t-ikz}, \quad (10)$$

$$\rho_{51} = \sum_{n=0}^{\infty} \rho_{51}^{(2n+1)} e^{in\zeta t+i(2n+1)kz} + \sum_{n=-\infty}^{0} \rho_{51}^{(2n-1)} e^{i(n-1)\zeta t+i(2n-1)kz}, \quad (11)$$

and substitute these into the Bloch equations (4)–(7). After substitution we obtain an infinite series of coherences spatially varying as $e^{\pm i(2n+1)kz}$ and $e^{\pm i2nkz}$ with $n \geqslant 0$. For practical purposes this series can be truncated for a suitable $n > n_{\max}$ determined by the temperature of the medium or the relative detuning $|\zeta|$ [44,45]. While $n_{\max} = 0$ for a room-temperature medium, this approximation can also be done for cold atoms when the relative detunings of the counterpropagating control fields or the corresponding Doppler shifts $\pm 2nkv_{\text{atom}}$ of the coherences $\rho_{21}^{\pm 2n}$ are much larger than the EIT transparency window width $\Delta\omega_{\text{EIT}}$ [44,45]. We therefore obtain for the Maxwell-Bloch equations describing the propagation dynamics

$$\frac{\partial}{\partial t}\rho_{21}^{\pm(2n)} = -\left[\frac{\gamma_{21}}{2} - i(\delta \mp \Delta_n^{+})\right]\rho_{21}^{\pm(2n)} + \frac{i}{2}\Omega_c^{+*}\rho_{31}^{(\pm 2n+1)} + \frac{i}{2}\Omega_c^{-*}\rho_{31}^{(\pm 2n-1)} + \frac{i}{2}\tilde{S}_{25}\Omega_c^{+*}\rho_{51}^{(\pm 2n+1)} + \frac{i}{2}\tilde{S}_{25}\Omega_c^{-*}\rho_{51}^{(\pm 2n-1)}, \quad (12)$$

$$\frac{\partial}{\partial t}\rho_{31}^{\pm(2n+1)} = -\left[\frac{\Gamma}{2} - i(\Delta_p^{+} \mp \Delta_n^{\pm})\right]\rho_{31}^{\pm(2n+1)} + \frac{i}{2}\Omega_p^{\pm}\delta_{n,0} + \frac{i}{2}\Omega_c^{\pm}\rho_{21}^{\pm(2n)} + \frac{i}{2}\Omega_c^{\mp}\rho_{21}^{\pm(2n+2)}, \quad (13)$$

$$\frac{\partial}{\partial t}\rho_{41}^{(\pm 1)} = -\left[\frac{\Gamma}{2} - i(\Delta_p^{\pm} - \Delta_{34})\right]\rho_{41}^{(\pm 1)} + \frac{i}{2}\tilde{S}_{14}\Omega_p^{\pm}, \quad (14)$$

$$\frac{\partial}{\partial t}\rho_{51}^{\pm(2n+1)} = -\left[\frac{\Gamma}{2} - i(\Delta_p^{+} - \Delta_{35} \mp \Delta_n^{\pm})\right]\rho_{51}^{\pm(2n+1)} + \frac{i}{2}\tilde{S}_{15}\Omega_p^{\pm}\delta_{n,0} + \frac{i}{2}\tilde{S}_{25}\Omega_c^{\pm}\rho_{21}^{\pm(2n)} + \frac{i}{2}\tilde{S}_{25}\Omega_c^{\mp}\rho_{21}^{\pm(2n+2)}, \quad (15)$$

$$\frac{1}{c}\frac{\partial}{\partial t}\Omega_p^{\pm} \pm \frac{\partial}{\partial z}\Omega_p^{\pm} = i\frac{\Delta\omega_{21}}{c}\Omega_p^{\pm} + i\frac{D_{\text{opt}}\,\Gamma}{2L}\left(\rho_{31}^{(\pm 1)} + \tilde{S}_{14}\rho_{41}^{(\pm 1)} + \tilde{S}_{15}\rho_{51}^{(\pm 1)}\right), \quad (16)$$

for $n \geqslant 0$ with $\Delta_n^{+} = n\zeta, \Delta_n^{-} = (n+1)\zeta$, the Kronecker delta $\delta_{n,0}$, $\Delta_p^{-} = \Delta_p^{+} + \zeta$, D_{opt} being the optical depth for the transition $|1\rangle \leftrightarrow |3\rangle$ and L being the medium length. We also accounted for a phase mismatch $(k_p^{+} - k_c^{+})c = \Delta\omega_{21} = 2\pi \times 6.835$ GHz due to the energy difference of the two ground states $|1\rangle$ and $|2\rangle$ and the perfect 1D geometry of the propagation inside the fiber [43,44].

We note that the time-dependent Stark shift Δ_S is included in the detunings $\Delta_c^{\pm}$ and the Doppler shifts $\pm kv_{\text{atom}}$ are included in the detunings $\Delta_{p,c}^{\pm}$. An average over the thermal velocity distribution for given temperature Θ can therefore be taken [44,45]. The ground-state decoherence rate $\gamma_{21} = \gamma_{\text{trd}} + \gamma_{\text{inh}}$ is determined by transit relaxation decay γ_{trd} (depending on the temperature Θ of the atoms inside the fiber) [48], and an effective contribution γ_{inh} due to the inhomogeneous broadening by the spatially varying control beams and atomic

density (see next section). We neglect the contribution of the relative linewidth $\gamma_{\rm lock}$ of the probe and control beams, since $\gamma_{\rm lock} \ll \gamma_{21}$. To further account for the radially inhomogeneous distributions of atomic density and Rabi frequencies, we also use effective Rabi frequencies $\Omega^{\rm eff} = \beta\Omega$ determined from simulated transmission spectra (see next section). We then numerically solve Eqs. (12)–(16) to simulate slow light, light storage and retrieval, and SLPs with $n_{\rm max} = 3$. Only the number of atoms $N_{\rm atom}$ inside the HCPCF and Θ were free parameters. The other parameters were initially chosen according to the measurements and were then allowed to be changed within the experimental uncertainties to best reproduce the measured data.

C. EIT transmission spectra

We calculate transmission spectra $T(\Delta_p^+)$ for the six-level system, displayed in Fig. 2 (level $|6\rangle$ is adiabatically eliminated) under EIT conditions with a single control field Ω_c^+ as follows. We set $\Omega_{p,c}^- = \Delta_{p,c}^- \equiv 0$ and we substitute $\Omega_{p,c}^+ = \Omega_{p,c}$ in the equations above. The Hamiltonian and the Bloch equations are therefore the same as in the previous section, however, with all couplings in the negative z direction set to zero.

For obtaining the stationary transmission, we derive the stationary solution of Eqs. (4)–(7), using the same initial conditions $\rho_{11}^{(0)} = 1$ and $\rho_{ij}^{(0)} = 0$ for all $(i,j) \neq (1,1)$ as before. From here we obtain the absorption coefficient for a *homogeneous* medium as

$$\alpha(\Delta_p^+) = A_{p4}\tilde{S}_{14}^2 + \frac{\left[A_{p3} + A_{p5}\tilde{S}_{15}^2 + BA_{p3}A_{p5}|\tilde{S}_{15} - \tilde{S}_{25}|^2\Omega_c^2\right]}{\left[1 + BA_{p3}|\Omega_c|^2 + BA_{p5}|\tilde{S}_{25}\Omega_c|^2\right]}, \tag{17}$$

where $A_{pj} = [\Gamma/2 - i(\Delta_p^+ - \xi_j)]^{-1}$; $j = 3,4,5$; $\xi_3 = 0$; $\xi_4 = \Delta_{34}$; $\xi_5 = \Delta_{35}$; and $4B = [\gamma_{21}/2 - i(\Delta_p^+ - \Delta_c^+ - \Delta_S)]^{-1}$. We here have re-introduced the Stark shift $\Delta_S = \Delta_S^+$ due to level $|F' = 3\rangle$.

The transmission is then given by

$$T(\Delta_p^+) = \exp\left[-\frac{\Gamma}{2} D_{\rm opt}\,\alpha(\Delta_p^+)\right], \tag{18}$$

with $D_{\rm opt} = n_0\,\sigma_{\rm atom}\,L$ where n_0 is the atomic density, $\sigma_{\rm atom}$ is the absorption cross section of the transition $|1\rangle \rightarrow |3\rangle$, and L is the length of the medium.

To include the radially inhomogeneous Rabi frequencies $\Omega(r)$ and atomic density $n(r)$ depending on the radial distance r from the fiber axis, we obtain the transmission through the fiber with cylindrical symmetry as follows. The Rabi frequencies $\Omega_{p,c}(r) = \Omega_{p,c}(0)\exp(-r^2/\sigma_{p,c}^2)$ with the measured mode field $1/e^2$ radius of the intensity $\sigma_{p,c}$ of the probe and control beams simply replaces the constant Rabi frequencies in Eq. (17). The radial atomic density distribution is $n(r) = n_0\exp(-r^2/\sigma_a^2)$, with the $1/e^2$ radius σ_a as determined by the temperature Θ of the atoms inside the far-off-resonant trap (FORT) potential of known depth [46].

The transmission through the *inhomogeneous* medium inside the fiber is then given by

$$T(\Delta_p^+,\Theta) = \exp\left[-\Gamma\frac{\sigma_{\rm atom}}{\sigma_{p,c}^2} L \iint n(r)\,p(v_{\rm atom}) \times \Omega_p(r)\alpha(r,\Delta_p^+)r\;dr\,dv_{\rm atom}\right] \tag{19}$$

with the Maxwell-Boltzmann distribution $p(v_{\rm atom})$ for a temperature Θ.

A comparison of the transmission spectra for homogeneous and inhomogeneous laser fields and medium, respectively, shows that the inhomogeneities can be included in the (homogeneous) 1D simulation by using effective control Rabi frequencies $\Omega_c^{\rm eff} = \beta\Omega_c$ and an additional decoherence rate $\gamma_{\rm inh} \propto \Omega_c^2, \Theta^2$ due to inhomogeneous broadening. For the values of Θ and Ω_c used in our experiment we have $\gamma_{\rm inh} > \gamma_{\rm trd}$.

The parameters β and $\gamma_{\rm inh}$ are determined by comparing the results of Eqs. (18) and (19) for the homogeneous/inhomogeneous cases with β and $\gamma_{\rm inh}$ included in the homogeneous transmission function. We then adjust β and $\gamma_{\rm inh}$ for all other parameters being identical, until the transmission of both spectra is the same within $<1\%$. As β and $\gamma_{\rm inh}$ depend on the temperature Θ and the control Rabi frequencies, they are determined for each of them individually in the range of our experimental parameters.

For simulating the pulse propagation through the medium under EIT conditions we either used a convolution of the probe pulse and the spectral transmission function $T(\Delta_p^+,\Theta)$ in three dimensions or we solved the 1D Maxwell-Bloch equations (12)–(16) using $\Omega_c^{\rm eff}$ and $\gamma_{\rm inh}$. The latter method was also used to simulate light storage and SLPs.

III. EXPERIMENTAL SETUP

A schematic overview of the experimental setup is shown in Fig. 3. We first loaded about $N_0 = 10^7$ rubidium atoms into a standard vapor cell magneto-optical trap (MOT) with rectangular coil geometry [49]. After a loading period of 1 s we transferred the atom cloud down towards the tip of a vertically oriented HCPCF (HC-800-02, NKT Photonics, core diameter $\sim$7 μm), located $\sim$5.5 mm away from the center of the MOT, by shifting the magnetic zero point of the MOT with an offset magnetic field. Simultaneously, we compressed the cloud by ramping up the current in the quadrupole coils of the MOT to achieve a gradient of 15 G/cm. To avoid density-limiting light-assisted collisions near the HCPCF, we used the so-called

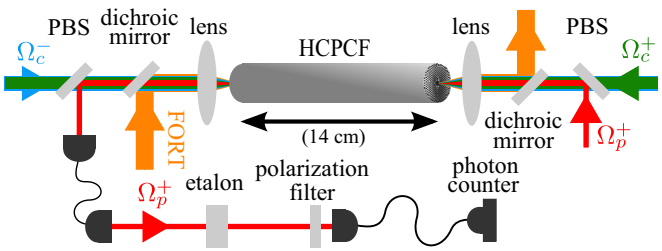

FIG. 3. Schematic experimental setup. PBS: polarizing beam splitter.

dark spot technique [50] to create a dark funnel for the atoms [38]. While the atom cloud was held above the fiber tip it could fall into a near Gaussian-shaped red-detuned FORT [46] located inside the HCPCF. The FORT was realized by coupling radiation at a wavelength of 855 nm and a power of 270 mW (corresponding to a trap depth of ∼5 mK) into the HCPCF. The FORT therefore prevented collisions of the laser-cooled rubidium atoms with the room-temperature fiber wall, allowing for guiding and a tight confinement of the atoms. With this setup, we were able to load up to 2.5% of the atoms into the HCPCF, resulting in a D_{opt} of up to 1000 [38]. The total number of atoms N_{atom} loaded into the fiber could be controlled by the power of the repumper beam tuned to the transition $|1\rangle \rightarrow |5\rangle$ which forms the dark funnel. The loading process of the HCPCF was repeated every 1.3 s.

For a 5-mK deep FORT a temperature around 450 μK of the atoms inside the HCPCF can be expected. However, due to an unresolved heating mechanism, the temperature varied day by day between $350\,\mu\mathrm{K} \leqslant \Theta \leqslant 1.1$ mK [37,38]. To avoid inhomogeneous broadening by the deep FORT, we modulated the trap depth with an on-off ratio of $\geqslant$14 dB and $\omega_{\mathrm{mod}} = 2\pi \times 250$ kHz. This was done by an acousto-optic modulator (AOM) placed between the diode laser and the tapered amplifier of our master oscillator power amplifier system [38]. Although the 90–20% fall time was 170 ns, the rf power of the AOM driver oscillator would decay with a time constant of 260 ns ($1/e$) thereafter leading to non-negligible ac Stark shifts during the measurements within the short measurement periods of $\tau_{\mathrm{meas}} \leqslant 3\,\mu$s. This effect was qualitatively observed for different commercial and home-built drivers. To overcome this problem we used an additional fast absorptive switch (MiniCircuits, ZYSWA-2-50DR) between oscillator and amplifier of the AOM driver. The resulting 90–10% fall and rise time was then 95 ns with a suppression of $\geqslant$14 dB of the FORT during the measurements. This is sufficient to reduce the trap depth to $<225\,\mu$K, which is below the temperature of the atoms, and to one-photon ac Stark shifts of less than 0.2Γ, where $\Gamma = 2\pi \times 6.07$ MHz is the excited-state linewidth. The modulation provided up to 50 measurement periods $\tau_{\mathrm{meas}} \leqslant 3\,\mu$s each, with insignificant losses.

Although the central part of the HCPCF was shielded from magnetic stray fields by a layer of μ metal, the regions within around 2 cm from the fiber tips were not shielded. We therefore observed a beating of the light storage retrieval efficiency due to the (decaying) quadrupole field of the MOT [51,52]. This effect could, however, be compensated by applying a suitable three-dimensional magnetic offset field following the procedure in Ref. [51]. This offset field had to be adjusted slightly day by day. To guarantee interaction with only the atoms inside the HCPCF during any of the here presented experiments, we switched off the magnetic field of the MOT 14 ms earlier and pumped the region above the fiber continuously with the repumper beam with a power of 600 μW and a $1/e^2$ diameter of 2 mm once the fiber was loaded. The atoms inside the HCPCF were optically pumped into level $|F = 1\rangle$ by the control laser.

Two external-cavity diode lasers locked [53] with a relative bandwidth of 8 kHz during an integration period of 3.5 s provided the probe and control fields. Both laser beams were launched with linear orthogonal polarizations into the HCPCF. Due to the typical birefringence of HCPCFs [54] and nonperfect input coupling [55] the light fields were elliptically polarized inside the fiber, with a degree of linear polarization of ∼90% after the fiber. Therefore we implemented the Λ scheme for EIT as shown in Fig. 1(b) with $|1\rangle = |5\,^2S_{1/2}, F = 1\rangle$, $|2\rangle = |5\,^2S_{1/2}, F = 2\rangle$, and $|3\rangle = |5\,^2P_{3/2}, F' = 1\rangle$. With these couplings effectively two independent Λ schemes for EIT are created while one of the Zeeman states in $|F = 1\rangle$ is never coupled by the probe.

In order to separate the weak probe field ($3.5\,\mathrm{pW} \leqslant P_{\mathrm{probe}} \leqslant 700$ pW) from the much stronger and exactly collinear forward control field ($50\,\mathrm{nW} \leqslant P_{\mathrm{control}} \leqslant 1.7\,\mu$W) after the HCPCF for detection with a photon counter (PerkinElmer, SPCM AQRH-12), we proceeded as follows. First, the light exiting the fiber was passing a polarization beam splitter. Then the light was spatially filtered by a single-mode fiber [37]. Finally we used a combination of a monolithic etalon, polarization filter, and a second spatial filter [56] by coupling the light into a single-mode fiber leading to the photon counter. This led to a detection efficiency of 10% for the probe and a relative extinction ratio of 64 dB for the control beam. We always kept the probe power low enough to fulfill $\Omega_p \ll \Omega_c$ and to have much smaller densities of the probe photons than the atoms, as required for DSP propagation [11]. We counted the output pulses of the SPCM either directly with a counterboard (NI, PCI-6602) or with a digital storage oscilloscope (Agilent, DSO1014A) followed by software analysis. For further details on the experimental setup we refer the reader to [38].

IV. RESULTS AND DISCUSSION

A. EIT

Figure 4(a) shows the transmission through the HCPCF as a function of probe laser detuning for two different D_{opt}. Each data point corresponds to $N_{\mathrm{avg}} = 50$ averages measured during a gate time of $\tau_g = 680$ ns. In the absence of EIT the medium can be rendered highly opaque over a broad frequency range depending on the number of atoms loaded into the fiber. The corresponding D_{opt} per atom was $D^*_{\mathrm{opt}} = 0.0037(6)$ for the transition used, in agreement with previous results [37]. By switching on the control beam during the measurement

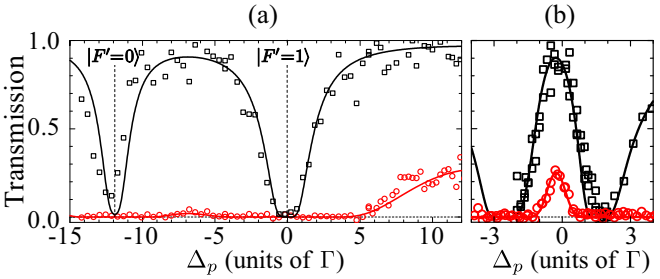

FIG. 4. (a) Experimental (symbols) and simulated (lines) transmission through the HCPCF filled with atoms for D_{opt} of 20 (black squares) and 400 (red circles) without control field. (b) EIT at resonance for the parameters D_{opt}=20, $\Omega_c^+ = 4.5\Gamma$, $\Delta_c^+ = 0.7\Gamma$, $\Theta = 550(50)\,\mu$K (black squares) and D_{opt}=400, $\Omega_c^+ = 6.1\Gamma$, $\Delta_c^+ = 1.8\Gamma$, $\Theta = 450(50)\,\mu$K (red circles).

for the same conditions, the typical transmission window of EIT appears [Fig. 4(b)]. The detuning $\Delta_c^+ > 0$ was here adjusted to compensate the two-photon ac Stark shift. The temperature of the medium was $\Theta = 500(100)\,\mu$K [$\gamma_{\rm trd} = 0.008(1)\Gamma$] according to the simulations based on Eq. (19). This is in agreement with the expected lower temperature limit for the ∼5-mK deep FORT. Whereas we observed almost complete transmission for a moderate $D_{\rm opt}$ (black squares), the maximum transmission reached only 25% for a high $D_{\rm opt}$ (red circles). According to our simulation, 30% of the absorption is due to incoherent absorption by level $|5\,^2P_{3/2}, F' = 0\rangle$ which is not coupled by the control due to selection rules. We therefore chose $D_{\rm opt} \lesssim 140$ for all following experiments to avoid a resonance overlap.

B. Slow light

Using the steep dispersion within the EIT transparency window, the group velocity v_g of a probe pulse can be significantly reduced as compared to the vacuum value c [2]. As the pulse is simultaneously spatially compressed by v_g/c, it can be stored efficiently inside a medium much shorter than the original pulse length. The temporal delay can be estimated by $\tau_d = \Gamma\, D_{\rm opt}/\,\Omega_c^2$ [11]. With the experimentally determined Ω_c (measuring the transmitted power and considering the losses of the optics) this allows one to determine the $D_{\rm opt}$ independently from the transmission spectra. Both results agree well within the experimental uncertainties. In Fig. 5(a) we show the delays of an incident probe pulse (black squares) for constant Ω_c^+ and varying $D_{\rm opt}$ ($N_{\rm avg} = 1250$, $\tau_g = 60$ ns). The delay increases linearly with the $D_{\rm opt}$ in accordance with the theoretical expectation (see inset). The probe pulse can be delayed by more than one pulse length, i.e., it can be compressed such that it completely fits inside the medium. We note that only by including the radially inhomogeneous profiles $\Omega_{p,c}(r)$ and $n(r)$ the simulations show good agreement with the measurements for realistic parameters (see Sec. II B).

C. Light storage and retrieval

By adiabatically switching off the control field while the probe pulse is inside the medium, we can now map the probe pulse onto a collective atomic excitation [2,12]. Switching on the same control field after a certain storage time leads to a retrieval of the probe field into its original direction. Figure 5(b) shows the incident probe pulse (black squares), the delayed pulse without storage (orange circles), and the retrieved pulses for different storage times $\Delta\tau$ (blue triangles, red diamonds, and green stars; $N_{\rm avg} = 1250$, $\tau_g = 60$ ns). The probe pulse is attenuated by 63% as it moves through the medium (orange circles). This attenuation cannot be solely attributed to decoherence by transit relaxation decay, but requires the inclusion of inhomogeneous broadening [$\gamma_{\rm inh} = 0.015(1)\Gamma$] by the control while $\Omega_c^+(t) \neq 0$ in the effective 1D simulation. Once the pulse is temporarily stored [while $\Omega_c^+(t) = 0$], it decays exponentially (black dashed line) with a decoherence rate $\gamma_{21} = 0.009(1)\Gamma$ dominated by transit relaxation decay ($\gamma_{\rm trd} = 0.008\Gamma$) for a temperature of 450(50) μK. We note that this exponential decay was achieved after careful suppression of the stray magnetic field [51]. Before, collapses and revivals

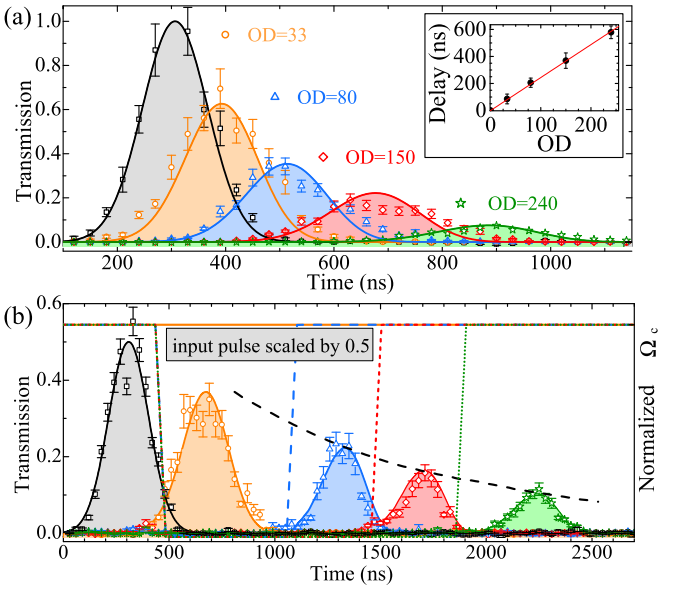

FIG. 5. Normalized transmission of a Gaussian input probe pulse (black squares) through the HCPCF. Symbols depict experimental data and lines simulations. The control Rabi frequencies are indicated by line segments. The time scales are different in both plots. (a) Slow light: The input pulse is delayed depending on the $D_{\rm opt}$ for $\Omega_c^+ = 3.8\Gamma$. $\Theta = 575(75)\,\mu$K, $\gamma_{21} = 0.037(3)\Gamma$. (b) Light storage: The input pulse is delayed by approximately one pulse width for constant Ω_c^+ (orange circles and line). The solid, dashed, and dotted lines represent $\Omega_c^+(t)$ with colors according to the respective transmission for different storage times of 0.6 μs (blue triangles) and 1 μs (red diamonds) with $D_{\rm opt}$=145(5), and a time of 1.4 μs (green stars) with $D_{\rm opt}$=195(5). $\Omega_c = 3.7\Gamma$, $\Theta = 450(50)\,\mu$K, $\gamma_{\rm trd} = 0.008(1)\Gamma$.

as in Ref. [52] were observed. The efficiency, defined as output-input pulse area, is $\eta = 23(5)\%$ for 0.6 μs of storage. This is about 2× (8×) larger than for similar measurements performed with nanofibers [52,57] (with similar decoherence rates) due to the larger $D_{\rm opt}$ but also larger inhomogeneous broadening. The latter one is also responsible for the lower efficiency as expected for free-space setups of comparable $D_{\rm opt}$ [3].

D. Stationary light pulses

Finally, we turn to the creation of SLPs with the use of two counterpropagating control fields. Figure 6 shows the transmission of an incident probe pulse (black squares) through the HCPCF when driven under slow light and SLP conditions ($N_{\rm avg} = 250$, $\tau_g = 100$ ns).

As before, Ω_c^+ was first adjusted (with $\Omega_c^- = 0$) to fit the probe pulse well into the medium (orange circles). Then the counterpropagating control (red dashed line) was applied as the probe pulse was inside the medium. During the time when the medium is driven by the two counterpropagating control fields the transmission through the fiber is significantly suppressed (red diamonds). Switching off the backward control field again retrieves the remaining coherence, i.e., a light pulse from the medium (see Fig. 6 inset). The retrieval efficiency is $\eta = 2.8(6)\%$ and occurs at times where there should not be any more coherence left inside the medium for a continuously propagating pulse. This is the typical

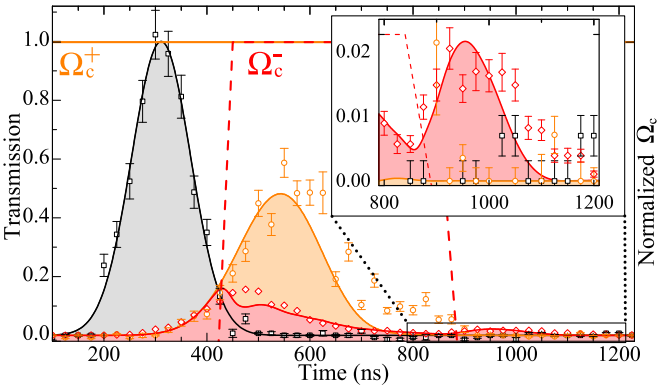

FIG. 6. Normalized transmission of a Gaussian input probe pulse (black squares) through the HCPCF. Symbols depict experimental data and lines simulations. The control Rabi frequencies are indicated by line segments. Slow light: $\Omega_c^+ = 2.6\Gamma$, $\Omega_c^- = 0$, $\gamma_{\rm inh} = 0.003(1)\Gamma$ (orange circles). SLP: $\Omega_c^+ = 2.6\Gamma$, $\Omega_c^- = 3.8\Gamma$, $\gamma_{\rm inh} = 0.012(1)\Gamma$ (red diamonds). $D_{\rm opt}$=53, $\Theta = 350(50)\,\mu$K, $\gamma_{\rm trd} = 0.006(1)\Gamma$, $\Delta_c^+ = +1.0\Gamma$, $\Delta_p^+ = +0.45\Gamma$, $\Delta_c^- = -2.5\Gamma$. The inset shows an enlarged version for $t > 800$ ns.

signature of SLPs at moderate $D_{\rm opt}$ when the probe pulse just fits inside the medium [13,14]. The transmitted light detected when $\Omega_c^{\pm}(t) \neq 0$ can be explained by the parts of the pulse near the edges of the medium leaking out due to diffusion [13,14]. This is also confirmed by the numerical simulation (red solid line). As the two-photon Doppler shifts $(k_p^{\pm} - k_c^{\mp})v$ were smaller than $\Delta\omega_{\rm EIT}$, we applied a relative detuning $(\Delta_c^+ - \Delta_c^-) = 3.5\Gamma > \Delta\omega_{\rm EIT} = 2.9\Gamma$ to avoid excitation of coherences suppressing the SLPs [14,44,45]. For $\Delta_c^- = \Delta_c^+$ no pulse could be retrieved, as expected for a cold medium [14]. Due to the ground-state frequency difference of $\Delta\omega_{21} = 2\pi \times 6.835$ GHz and the exact 1D alignment of all laser beams a phase mismatch is present which must be compensated by a two-photon detuning $\delta_{pm} = -\Delta\omega_{21} v_g/c$ [43]. If $\delta_{pm} \gtrsim \Delta\omega_{\rm EIT}$ this leads to strong attenuation of the SLPs. This effect becomes negligible for media of large $D_{\rm opt}$ and correspondingly large group delays; however, it has to be considered in our experiment. Therefore, we set the detunings $\Delta_{p,c}^+$ such that an effective negative two-photon detuning within the EIT window width was realized (taking into account the ac Stark shifts by the control). Without an initial two-photon detuning, no SLPs could be observed for our parameters. Unlike for phase-matched conditions [14], we obtained the largest retrieval efficiency for $\Omega_c^- \neq \Omega_c^+$. This is confirmed by numerical simulations for our parameters with comparable δ_{pm}, $\Delta\omega_{\rm EIT}$, and pulse bandwidth $\Delta\omega_p$. The simulations show that the ratio $\Omega_c^-/\Omega_c^+ \to 1$ for obtaining SLPs as $\Delta\omega_p, \delta_{pm} \ll \Delta\omega_{\rm EIT}$. Our explanation for this is as follows: The phase mismatch is relevant for the excitation of the backward propagating field Ω_p^- only, as $\Delta K^- = |\vec{k}_p^+ - \vec{k}_c^+ + \vec{k}_c^- - \vec{k}_p^-| \approx 2(k_p^+ - k_c^+)$ with $k_{p,c}^+ = |\vec{k}_{p,c}^+|$ and $\vec{k}_{p,c}^+ \approx -\vec{k}_{p,c}^-$. For Ω_p^+ it is not relevant, as $\Delta K^+ = k_p^+ - k_c^+ + k_c^+ - k_p^+ = 0$ when the probe pulses are sent into the medium with the forward control being present. When not all frequencies of the probe pulse can be phase matched, the resulting suppression of the backward propagating field has to be compensated by a stronger coupling Ω_c^- to achieve an effective SLP. Simulations show that for $\Delta\omega_p$, $\delta_{pm} \ll \Delta\omega_{\rm EIT}$ good phase matching for all probe frequencies becomes possible and SLPs are formed again for balanced coupling.

V. OUTLOOK

In view of the goal of achieving efficient light storage and NLO interactions at the single-photon limit the following steps have to be taken:

(i) The relative extinction ratio of probe and control beams must be improved by ∼20 dB to reach the interesting single-photon regime. This is technically feasible by improved polarization filtering as shown for a similar filter [56].

(ii) Incoherent (off-resonant) absorption must be suppressed to allow for larger $D_{\rm opt}$ and hence larger light storage and SLP efficiencies. This can be achieved by using the D_1 instead of the D_2 line with a fewer number of excited states and the approximately fivefold larger hyperfine splitting [47].

(iii) Inhomogeneous broadening by the control itself must be reduced to maintain the condition $\Delta\omega_{\rm EIT} \gg \gamma_{21}$ also at larger $D_{\rm opt}$. Cooling the atoms *inside* the 1D FORT, as, e.g., demonstrated in Refs. [58,59], will reduce decoherence, inhomogeneous broadening, and heating-induced losses, resulting in larger probe transmission, $D_{\rm opt}$, and longer averaging times. Collisional thermalization in three dimensions will be possible at our present atomic densities of 10^{12} cm^{-3} [38] resulting in temperatures well below the Doppler limit [59]. By applying, e.g., the cooling technique in Ref. [59] inside the fiber (to reduce inhomogeneous broadening) and the technique shown in Ref. [60] (to suppress decoherence), the light storage efficiency and period could be significantly extended also inside a HCPCF, approaching the values known from free-space experiments. According to our simulation the efficiency for SLPs would be already one order of magnitude larger than the value presented here by using the D_1 line with an $D_{\rm opt}$ of 500 and by cooling the atoms to 50 μK. Finally, we estimate the feasibility to observe NLO effects at the few-photon level with our setup as, e.g., discussed in Ref. [15]. For $D_{\rm opt} \lesssim 1000$, as demonstrated in our current and previous work [38], and with $D_{\rm opt}^* = 0.0037(6)$ we have $D_{\rm opt} \times D_{\rm opt}^* \lesssim 3.7$. With at least the two improvements (i) and (ii) mentioned above and by extrapolating the data shown in Ref. [15] to larger $D_{\rm opt}$, NLO interactions with dissipative couplings should be observable.

VI. SUMMARY

In conclusion, we demonstrated the creation of SLPs and narrowband light storage using EIT inside a HCPCF. Good agreement between numerical simulations and the experiments was found when considering the radially inhomogeneous laser beams and atomic density inside the fiber. The light storage efficiency was limited to around 23(5)% at a decoherence rate of $\gamma_{21} = 2\pi \times 64$ kHz dominated by transit relaxation decay. The minimum number of photons per pulse was ∼70 and the $D_{\rm opt}$ per atom was $D_{\rm opt}^* = 0.0037(6)$ for the transition used. We discussed several strategies for improving the experiment towards the goal of reaching linear and NLO interactions at the few-photon regime. Our work therefore paves the way towards a multitude of experiments requiring strong light-matter interactions in the field of quantum and nonlinear optics.

ACKNOWLEDGMENTS

The authors thank M. Szarafanowicz and Z. Zhou for technical assistance, T. Walther for providing us with a high-bandwidth ultra-low-noise current driver, and B.W. Shore, R. Walser, and M. Fleischhauer for fruitful discussions. The research leading to these results has received funding from the Deutsche Forschungsgemeinschaft and the European Union Seventh Framework Programme (FP7/2007-2013) under Grant No. PCIG09-GA-2011-289305.

[1] A.V. Gorshkov, A. André, M. D. Lukin, and A. S. Sørensen, Phys. Rev. A **76**, 033805 (2007).
[2] M. Fleischhauer, A. Imamoglu, and J. Marangos, Rev. Mod. Phys. **77**, 633 (2005).
[3] Y. H. Chen, M. J. Lee, I. Chung Wang, S. Du, Y. F. Chen, Y. C. Chen, and I. A. Yu, Phys. Rev. Lett. **110**, 083601 (2013).
[4] D. Schraft, M. Hain, N. Lorenz, and T. Halfmann, Phys. Rev. Lett. **116**, 073602 (2016).
[5] G. Hétet, J. J. Longdell, A. L. Alexander, P. K. Lam, and M. J. Sellars, Phys. Rev. Lett. **100**, 023601 (2008).
[6] Y.-W. Cho, G. T. Campbell, J. L. Everett, J. Bernu, D. B. Higginbottom, M. T. Cao, J. Geng, N. P. Robins, P. K. Lam, and B. C. Buchler, Optica **3**, 100 (2016).
[7] D. Chang, V. Vuletic, and M. Lukin, Nat. Photon. **8**, 685 (2014).
[8] G. Heinze, C. Hubrich, and T. Halfmann, Phys. Rev. Lett. **111**, 033601 (2013).
[9] Y.-F. Hsiao, P.-J. Tsai, H.-S. Chen, S.-X. Lin, C.-C. Hung, C.-H. Lee, Y.-H. Chen, Y.-F. Chen, I. A. Yu, and Y.-C. Chen, arXiv:1605.08519.
[10] M. Fleischhauer and M. D. Lukin, Phys. Rev. Lett. **84**, 5094 (2000).
[11] M. Fleischhauer and M. D. Lukin, Phys. Rev. A **65**, 022314 (2002).
[12] C. Liu, Z. Dutton, C. Behroozi, and L. Hau, Nature (London) **409**, 490 (2001).
[13] M. Bajcsy, A. Zibrov, and M. Lukin, Nature (London) **426**, 638 (2003).
[14] Y. W. Lin, W. T. Liao, T. Peters, H. C. Chou, J. S. Wang, H. W. Cho, P. C. Kuan, and I. A. Yu, Phys. Rev. Lett. **102**, 213601 (2009).
[15] M. Hafezi, D. E. Chang, V. Gritsev, E. Demler, and M. D. Lukin, Phys. Rev. A **85**, 013822 (2012).
[16] A. André, M. Bajcsy, A. S. Zibrov, and M. D. Lukin, Phys. Rev. Lett. **94**, 063902 (2005).
[17] Y. H. Chen, M. J. Lee, W. Hung, Y. C. Chen, Y. F. Chen, and I. A. Yu, Phys. Rev. Lett. **108**, 173603 (2012).
[18] D. Chang, V. Gritsev, G. Morigi, V. Vuletić, M. Lukin, and E. Demler, Nat. Phys. **4**, 884 (2008).
[19] M. Kiffner and M. J. Hartmann, Phys. Rev. A **81**, 021806 (2010).
[20] D. G. Angelakis, M. Huo, E. Kyoseva, and L. C. Kwek, Phys. Rev. Lett. **106**, 153601 (2011).
[21] H. Kimble, Nature (London) **453**, 1023 (2008).
[22] D. G. Angelakis, M.-X. Huo, D. Chang, L. C. Kwek, and V. Korepin, Phys. Rev. Lett. **110**, 100502 (2013).
[23] Y.-F. Hsiao, H.-S. Chen, P.-J. Tsai, and Y.-C. Chen, Phys. Rev. A **90**, 055401 (2014).
[24] T. Peyronel, O. Firstenberg, Q. Liang, S. Hofferberth, A. Gorshkov, T. Pohl, M. Lukin, and V. Vuletić, Nature (London) **488**, 57 (2012).
[25] Y. Dudin and A. Kuzmich, Science **336**, 887 (2012).
[26] O. Firstenberg, T. Peyronel, Q. Liang, A. Gorshkov, M. Lukin, and V. Vuletić, Nature (London) **502**, 71 (2013).
[27] J. Pritchard, K. Weatherill, and C. Adams, Annu. Rev. Cold Atoms Mol. **1**, 301 (2013).
[28] K. Birnbaum, A. Boca, R. Miller, A. Boozer, T. Northup, and H. Kimble, Nature (London) **436**, 87 (2005).
[29] B. Dayan, A. Parkins, T. Aoki, E. Ostby, K. Vahala, and H. Kimble, Science **319**, 1062 (2008).
[30] A. Goban, C. Hung, S. Yu, J. Hood, J. Muniz, J. Lee, M. Martin, A. McClung, K. Choi, D. Chang, O. Painter, and H. Kimble, Nat. Commun. **5**, 3808 (2014).
[31] A. Goban, C. L. Hung, J. D. Hood, S. P. Yu, J. A. Muniz, O. Painter, and H. J. Kimble, Phys. Rev. Lett. **115**, 063601 (2015).
[32] A. Goban, K. S. Choi, D. J. Alton, D. Ding, C. Lacroûte, M. Pototschnig, T. Thiele, N. P. Stern, and H. J. Kimble, Phys. Rev. Lett. **109**, 033603 (2012).
[33] S. T. Dawkins, R. Mitsch, D. Reitz, E. Vetsch, and A. Rauschenbeutel, Phys. Rev. Lett. **107**, 243601 (2011).
[34] S. Ghosh, A. R. Bhagwat, C. K. Renshaw, S. Goh, A. L. Gaeta, and B. J. Kirby, Phys. Rev. Lett. **97**, 023603 (2006).
[35] C. A. Christensen, S. Will, M. Saba, G. B. Jo, Y. I. Shin, W. Ketterle, and D. Pritchard, Phys. Rev. A **78**, 033429 (2008).
[36] S. Vorrath, S. Möller, P. Windpassinger, K. Bongs, and K. Sengstock, New J. Phys. **12**, 123015 (2010).
[37] M. Bajcsy, S. Hofferberth, T. Peyronel, V. Balic, Q. Liang, A. S. Zibrov, V. Vuletic, and M. D. Lukin, Phys. Rev. A **83**, 063830 (2011).
[38] F. Blatt, T. Halfmann, and T. Peters, Opt. Lett. **39**, 446 (2014).
[39] K. T. Kaczmarek, M. R. Sprague, S. Kolthammer, A. Feizpour, P. M. Ledingham, B. Brecht, E. Poem, I. A. Walmsley, J. Nunn, D. J. Saunders, M. R. Sprague, W. S. Kolthammer, A. Feizpour, P. M. Ledingham, B. Brecht, E. Poem, I. A. Walmsley, and J. Nunn, Opt. Lett. **40**, 5582 (2015).
[40] A. D. Slepkov, A. R. Bhagwat, V. Venkataraman, P. Londero, and A. L. Gaeta, Opt. Express **16**, 18976 (2008).
[41] M. R. Sprague, P. S. Michelberger, T. F. M. Champion, D. G. England, J. Nunn, X.-M. Jin, W. S. Kolthammer, A. Abdolvand, P. S. J. Russell, and I. A. Walmsley, Nat. Photon. **8**, 287 (2014).
[42] M. Bajcsy, S. Hofferberth, V. Balic, T. Peyronel, M. Hafezi, A. S. Zibrov, V. Vuletic, and M. D. Lukin, Phys. Rev. Lett. **102**, 203902 (2009).
[43] F. Zimmer, A. André, M. Lukin, and M. Fleischhauer, Opt. Commun. **264**, 441 (2006).
[44] J. H. Wu, M. Artoni, and G. C. La Rocca, Phys. Rev. A **82**, 013807 (2010).
[45] T. Peters, S. W. Su, Y. H. Chen, J. S. Wang, S. C. Gou, and I. A. Yu, Phys. Rev. A **85**, 023838 (2012).
[46] R. Grimm, M. Weidemüller, and Y. Ovchinnikov, Adv. At. Mol. Opt. Phys. **42**, 95 (2000).
[47] D. A. Steck, Rubidium 87 D Line Data, available online at http://steck.us/alkalidata (revision 2.1.5, 13 January 2015).

[48] J. Sagle, R. Namiotka, and J. Huennekens, J. Phys. B **29**, 2629 (1996).
[49] T. Peters, B. Wittrock, F. Blatt, T. Halfmann, and L. P. Yatsenko, Phys. Rev. A **85**, 063416 (2012).
[50] W. Ketterle, K. B. Davis, M. A. Joffe, A. Martin, and D. E. Pritchard, Phys. Rev. Lett. **70**, 2253 (1993).
[51] T. Peters, Y. Chen, J. Wang, Y. Lin, and I. Yu, Opt. Express **17**, 6665 (2009).
[52] B. Gouraud, D. Maxein, A. Nicolas, O. Morin, and J. Laurat, Phys. Rev. Lett. **114**, 180503 (2015).
[53] S. Bell, D. Heywood, J. White, J. Close, and R. Scholten, Appl. Phys. Lett. **90**, 171120 (2007).
[54] G. Statkiewicz, T. Martynkien, and W. Urbanczyk, Opt. Commun. **255**, 175 (2005).
[55] X. Chen, M.-J. Li, N. Venkataraman, M. T. Gallagher, W. A. Wood, A. M. Crowley, J. P. Carberry, L. A. Zenteno, and K. W. Koch, Opt. Express **12**, 3888 (2004).
[56] P. Palittapongarnpim, A. MacRae, and A. Lvovsky, Rev. Sci. Instrum. **83**, 066101 (2012).
[57] C. Sayrin, C. Clausen, B. Albrecht, P. Schneeweiss, and A. Rauschenbeutel, Optica **2**, 353 (2015).
[58] T. Peyronel, M. Bajcsy, S. Hofferberth, V. Balic, M. Hafezi, Q. Liang, A. Zibrov, V. Vuletic, and M. Lukin, IEEE J. Sel. Top. Quantum Electron. **18**, 1747 (2012).
[59] S. L. Winoto, M. T. DePue, N. E. Bramall, and D. S. Weiss, Phys. Rev. A **59**, R19 (1999).
[60] Y. O. Dudin, L. Li, and A. Kuzmich, Phys. Rev. A **87**, 031801 (2013).